Research Square

Preprints are preliminary reports that have not undergone peer review.
They should not be considered conclusive, used to inform clinical practice,
or referenced by the media as validated information.

Paeoniflorin suppresses ovarian cancer cell growth alongside altered TM4SF1 expression and cAMP signalling

Jing Zhang
1. Affiliated Xiaoshan Hospital, Hangzhou Normal University,

Yujie Chen
1. Affiliated Xiaoshan Hospital, Hangzhou Normal University,

Junjie Hong
Zhejiang Cancer Hospital

Wangang Gong
Zhejiang Cancer Hospital

Zhangguo Ying
Ningbo University

Aijun Yu
Zhejiang Cancer Hospital

Guangyi Jiang
jianggy@zjcc.org.cn

Zhejiang Cancer Hospital

Research Article

Keywords: paeoniflorin, ovarian cancer, TM4SF1, cAMP signalling, apoptosis

Posted Date: November 25th, 2026

DOI: https://doi.org/10.21203/rs.3.rs-11487568/v1

License: This work is licensed under a Creative Commons Attribution 4.0 International License.
Read Full License

Additional Declarations: No competing interests reported.

Paeoniflorin suppresses ovarian cancer cell growth alongside altered TM4SF1 expression and cAMP signalling

Jing Zhang1,*, Yujie Chen1,*, Junjie Hong2,3,*, Wangang Gong2,3, Zhangguo Ying4, Aijun Yu2,3,✉ and Guangyi Jiang2,3,✉

1 Affiliated Xiaoshan Hospital, Hangzhou Normal University, Zhejiang, China

2 Zhejiang Cancer Hospital, Hangzhou, Zhejiang 310022, China

3 Hangzhou Institute of Medicine, Chinese Academy of Sciences, Hangzhou, Zhejiang 310018, China

4 Ningbo University, Ningbo, Zhejiang 310018, China

*These authors contributed equally to this work.

†Correspondence: Mengmeng Shi (m18768109380@163.com)

Jing Zhang: 15888855132@163.com

Yujie Chen: cyjsc.student@sina.com

Junjie Hong: weihb@zjcc.org.cn

Wangang Gong: gongwg@zjcc.org.cn

Guangyi Jiang: jianggy@zjcc.org.cn

Zhangguo Ying: 19817585135@163.com

Mengmeng Shi: m18768109380@163.com

Abstract

Paeoniflorin (PF) is a chemically defined constituent of medicinal preparations derived from Paeonia species. Its effects on ovarian cancer phenotypes and associated signalling responses remain incompletely characterised. Here, we examined PF in SKOV3 and A2780 cells and assessed accompanying molecular changes. Chemical profiling and constituent comparisons provided the rationale for selecting PF from Erzhimaoling decoction (EZMLD). PF reduced cell viability, colony formation, migration-associated measurements and total sphere area. Treatment also increased apoptosis-associated staining, altered cell-cycle distribution and reduced the EdU-to-nuclear fluorescence intensity ratio. These responses coincided with lower TM4SF1 protein and mRNA expression and higher intracellular cyclic adenosine monophosphate (cAMP). Cell-based measurements showed a lower phosphorylated CREB-to-total CREB ratio, despite increased cAMP and PKA-associated assay signals. In OVCAR3 xenografts, PF treatment was associated with lower tumour volumes and lower tumour-tissue TM4SF1 measurements. Together, these observations support further investigation of PF and its associated TM4SF1 and cAMP responses in ovarian cancer. They do not establish direct TM4SF1 targeting, causal mediation by cAMP or exclusive responsibility of PF for the activity of EZMLD.

Keywords: paeoniflorin; ovarian cancer; TM4SF1; cAMP signalling; apoptosis

Introduction

Recurrence and acquired drug resistance remain major obstacles to effective ovarian cancer treatment[1,2]. Preclinical models can identify candidate interventions, but their interpretation depends on how closely they represent the disease[3]. Chemically defined natural products offer a way to examine individual pharmacological effects within the broader study of medicinal preparations[4].

EZMLD is an eight-herb preparation that includes Bai Shao (Paeonia lactiflora Pall.). Previous experiments reported antitumour activity of EZMLD in ovarian cancer models[5]. Chemical profiling and constituent comparisons in the present study prompted us to examine PF. PF has shown experimental activity in other cancer models[6], but its contribution to the effects of EZMLD remains unresolved.

TM4SF1 is a transmembrane-4 L6 family protein implicated in malignant cellular behaviour. In ovarian cancer cells, TM4SF1 silencing reduced migration and invasion without detectable effects on proliferation or cell-cycle distribution[7]. Studies in colorectal and lung cancers linked TM4SF1 to Wnt/β-catenin and DDR1–Akt/ERK–mTOR signalling, respectively[8,9]. These findings make TM4SF1 a candidate for examining treatment responses, but do not establish its role in PF-associated phenotypic changes.

cAMP regulates cellular responses through effectors that include protein kinase A (PKA) and exchange proteins directly activated by cAMP (EPAC1/2)[10,11]. Signalling specificity depends on local organisation by A-kinase anchoring proteins and phosphodiesterases[11,12]. In ovarian cancer models, roflumilast increased mitochondrial ferritin expression and inhibited tumour growth through cAMP–PKA–CREB signalling[13]. By contrast, cAMP–CREB1 hyperactivation was associated with platinum resistance, and inhibiting CREB1 phosphorylation restored platinum sensitivity[14]. These contrasting observations underscore the context dependence of cAMP responses. Whole-cell cAMP measurements alone cannot define downstream CREB activity or identify an upstream drug target[11,12].

We therefore examined PF-associated cellular phenotypes alongside TM4SF1 expression and cAMP-related responses in ovarian cancer models. We measured viability, colony formation, migration-associated endpoints, sphere area, apoptosis-associated staining and cell-cycle distribution. Molecular analyses assessed TM4SF1 abundance and ERK, STAT3 and CREB phosphorylation. Xenograft experiments provided additional tumour-tissue and tolerability-related measurements. This design characterised concurrent treatment responses without assuming a direct interaction between PF and TM4SF1.

Materials and methods

Cell culture and reagents

Human SKOV3 and A2780 ovarian cancer cells were reported as obtained from the American Type Culture Collection. SKOV3 cells were maintained in McCoy's 5A medium (Gibco, 16600082), and A2780 cells in RPMI-1640 medium (Gibco, 11875093). Both media contained 10% foetal bovine serum (Gibco, 10099141) and 1% penicillin–streptomycin (Gibco, 15140122). Cells were incubated at 37 °C in a humidified atmosphere containing 5% CO_2.

Paeoniflorin preparation and treatment

PF (CAS 23180-57-6; $C_{23}H_{28}O_{11}$; molecular weight, 480.46 g/mol) was listed as purchased from the Shanghai Institute of Chinese Materia Medica (HY-N0293). The reported batch purity was 98.94% by high-performance liquid chromatography (HPLC). Identity was assessed by comparing the retention time with a PF reference standard. The standard was obtained from the National Institutes for Food and Drug Control (batch 110736-202548; assigned content, 98.9%).

The principal cell-treatment concentration was 50 μM PF. Concentration series are specified in the corresponding figures. A 20 mM stock solution was prepared in phosphate-buffered saline (PBS), aliquoted and stored at −20 °C protected from light. Repeated freeze–thaw cycles were avoided, and working solutions were prepared on the day of use. At 50 μM PF, the final PBS concentration was 0.25% (v/v). Vehicle controls received the corresponding volume of PBS. For animal experiments, PF was prepared in PBS and passed through a 0.22-μm filter before intraperitoneal administration.

The reported primary antibodies included anti-TM4SF1 (Abcam, ab184268), anti-p-CREB (Ser133; Cell Signaling Technology, 9198S) and anti-β-actin (Proteintech, 60004-1-Ig). Entries for a PKA-related antibody (9624S) and an adenylyl cyclase antibody (13905-1-AP) require correction against the original reagent records. Secondary antibodies included HRP-conjugated goat anti-rabbit IgG (7074S) and goat anti-mouse IgG (7076S; Cell Signaling Technology). Alexa Fluor 488-conjugated donkey anti-rabbit IgG (Invitrogen, A21206) was used for fluorescence detection. The reported secondary-antibody dilutions were 1:5,000 for HRP conjugates and 1:500 for the fluorescent conjugate.

Animal models

Female BALB/c nude mice, aged 4–6 weeks, were obtained from Beijing Vital River Laboratory Animal Technology. The reported animal approval was issued by Zhejiang Cancer Hospital (2025-10-013). OVCAR3 cells (5×10^6 per mouse) were injected subcutaneously into the right flank. At approximately 100 mm^3 tumour volume, mice were allocated to vehicle-control or PF groups (n = 6 per group). Allocation was reported to use a computer-generated random-number table.

PF was prepared at 5.0 mg/mL in PBS (pH 7.2–7.4), passed through a 0.22-μm filter and used on the day of preparation. The reported regimen was 50 mg/kg by intraperitoneal injection once daily for 14 days. An injection volume of 10 mL/kg corresponded to 0.2 mL for a 20-g

mouse. Vehicle-control mice received the same volume of PBS on the same schedule. Injection timing and operator were matched between groups.

Tumour length (L) and width (W) were reported as measured every 2 days. Volume was calculated as $V = 0.5 \times L \times W^2$. Measurements were reported to be performed by an investigator blinded to group allocation. Each mouse received an individual code, with group identities concealed until data compilation and analysis.

The reported study endpoint was completion of treatment or a mean control-group tumour volume exceeding 1,500 mm^3, whichever occurred first. No animals were reported as excluded from the final analysis. Individual humane endpoints included tumour volume above 1,500 mm^3 or body-weight loss of at least 20% from baseline. Other criteria included ulceration or necrosis affecting more than 10% of the tumour surface. Persistent severe lethargy, hunched posture or impaired food or water access for more than 48 h were also listed. Mice meeting an endpoint were reported as euthanised by carbon dioxide inhalation followed by cervical dislocation.

Ethics approval

All animal experimental procedures were approved by the Institutional Animal Care and Use Committee (IACUC) of Zhejiang cancer hospital (Approval No. (2025-10-013)) and were conducted in strict accordance with the Guide for the Care and Use of Laboratory Animals.

Consent to participate

Not applicable. (This study does not involve human participants, human data, or human tissue.)

Cell viability assay

Cells were seeded in 96-well plates at 5×10^3 cells per well. After attachment, the medium was replaced with fresh medium containing PF at the indicated concentrations. At the specified time points (24, 48 or 72 h), 10 μL of CCK-8 reagent was added per well. Plates were incubated for 2 h before absorbance was measured at 450 nm using a BioTek Synergy H1 reader. Cell viability was expressed relative to control wells[15].

Colony formation assay

Cells were seeded in six-well plates at 500 cells per well and cultured in PF-containing medium. Medium was replaced every 3 days. After 10–14 days, colonies were fixed with 4% paraformaldehyde and stained with 0.1% crystal violet. Colonies containing more than 50 cells were counted[16].

Wound-healing assay

Confluent monolayers were scratched using a 200-μL pipette tip[17]. Detached cells were removed by washing with PBS. Cells were then maintained in medium containing 1% foetal bovine serum and PF. Images were acquired at 0 and 24 h, and wound closure was quantified using ImageJ[18].

Reverse-transcription quantitative PCR

Total RNA was extracted using TRIzol, and cDNA was synthesised using PrimeScript RT Master Mix (Takara, RR047A). Quantitative PCR used SYBR Premix Ex Taq II (Takara, RR820A) and a QuantStudio 5 system (Applied Biosystems). Expression was normalised to *GAPDH* and analysed using the reported $2^{-\Delta\Delta Ct}$ method[19].

The reported primer sequences are listed below.

TM4SF1

Forward: 5'-ATGGCCTTCGTGCTCATC-3'
Reverse: 5'-TCAGCCACAGAGGTAGTC-3'

CDH1 (E-cadherin)

Forward: 5'-CGAGAGCTACACGTTCACGG-3'
Reverse: 5'-GGGTGTCGAGGGAAAAATAGG-3'

FOS

Forward: 5'-CCCAGTCAGAGTCACCCAGC-3'
Reverse: 5'-AGTCCGTGCAGAAGTCCTGA-3'

NR4A1

Forward: 5'-TGTGCCAGTCTAGGTCAGCC-3'
Reverse: 5'-CAGCATCTTGAGCCTGCACT-3'

IRS2

Forward: 5'-TGGATGACCCAGTACGAGCA-3'
Reverse: 5'-TCCAGGTAGGCACAGTCACC-3'

CCND1

Forward: 5'-GCTGCGAAGTGGAAACCATC-3'
Reverse: 5'-CCTCCTTCTGCACACATTTGAA-3'

CDK2

Forward: 5'-GTGAGCATGGAGACCTTCGA-3'
Reverse: 5'-TTCATCCAGGGGAGGTACAAC-3'

BAX

Forward: 5'-CCCGAGAGGTCTTTTTCCGAG-3'
Reverse: 5'-CCAGCCCATGATGGTTCTGAT-3'

BCL2

Forward: 5'-GGTGGGGTCATGTGTGTGG-3'
Reverse: 5'-CGGTTCAGGTACTCAGTCATCC-3'

GAPDH (internal control)

Forward: 5'-GGAGCGAGATCCCTCCAAAAT-3'
Reverse: 5'-GGCTGTTGTCATACTTCTCATGG-3'

Western blotting

Cells were lysed in RIPA buffer containing protease and phosphatase inhibitors. Protein concentrations were measured using a bicinchoninic acid (BCA) assay. Equal protein amounts (20–30 μg) were separated by SDS–PAGE and transferred to PVDF membranes (Millipore). Membranes were blocked with 5% non-fat milk and incubated with primary antibodies overnight at 4 °C. Following incubation with HRP-conjugated secondary antibodies, signals

were developed using enhanced chemiluminescence (Millipore). Band intensities were quantified using ImageJ[18].

Immunofluorescence and immunohistochemistry

For cell immunofluorescence, samples were fixed with 4% paraformaldehyde, permeabilised with 0.1% Triton X-100 and blocked with 5% bovine serum albumin. Anti-TM4SF1 antibody was applied at 1:200 overnight at 4 °C. Alexa Fluor 488-conjugated secondary antibody was used for detection, and nuclei were counterstained with DAPI. Images were acquired using a Zeiss LSM 880 confocal microscope.

For immunohistochemistry, paraffin sections were deparaffinised, subjected to antigen retrieval and incubated with primary antibodies. Signals were developed using HRP-conjugated secondary antibodies and diaminobenzidine, followed by haematoxylin counterstaining. Staining intensity and positivity were reported as scored independently by two pathologists blinded to group allocation.

Co-immunoprecipitation

Cells were lysed in NP-40 buffer containing protease inhibitors. Precleared lysates were incubated overnight at 4 °C with anti-TM4SF1, anti-adenylyl cyclase or control IgG. Protein A/G magnetic beads were then added, followed by extensive washing. Bound proteins were eluted in SDS loading buffer, boiled and analysed by immunoblotting.

Additional in vivo metastasis procedures

For lung-metastasis experiments, luciferase-expressing OVCAR3 cells (1×10^6 in 100 µL PBS) were injected intravenously. Pulmonary tumour burden was monitored weekly using an IVIS Spectrum imaging system. For peritoneal dissemination, cells (5×10^5 in 200 µL PBS) were injected intraperitoneally, and abdominal bioluminescence was measured.

Apoptosis analysis

Apoptosis-associated staining was assessed by Annexin V–FITC and propidium iodide (PI) flow cytometry[20]. Both adherent and floating cells were collected after treatment. Adherent cells were detached using EDTA-free trypsin. Cells were washed twice with cold PBS and resuspended in binding buffer at 1×10^6 cells/mL. Each sample received 5 µL Annexin V–FITC and 5 µL PI solution (20 µg/mL). After incubation for 15 min at room temperature in the dark, samples were analysed within 1 h. At least 1×10^4 events were acquired per sample.

Cell-cycle analysis

Cells were collected, washed with cold PBS and fixed by dropwise addition of prechilled 70% ethanol with gentle agitation. Following overnight fixation at −20 °C, ethanol was removed by centrifugation. Cells were washed with PBS and incubated with RNase A (100 µg/mL) for 30 min at 37 °C. Samples were stained with PI (50 µg/mL) in 0.1% Triton X-100 for 30 min at room temperature in the dark. DNA content was analysed by flow cytometry, with at least 2×10^4 events acquired per sample[21].

EdU incorporation assay

EdU labelling was assessed using a click chemistry assay[22]. Cells were seeded on coverslips or in 96-well plates. At the end of treatment, EdU was added at 10 μM, followed by incubation for 2 h at 37 °C.

Cells were fixed with 4% paraformaldehyde for 15 min and permeabilised with 0.3% Triton X-100 for 15 min. The fluorescent azide reaction was performed for 30 min in the dark according to the kit instructions. Nuclei were reported as counterstained with Hoechst 33342 (5 μg/mL) for 10 min.

Images were acquired using fluorescence or confocal microscopy, with five randomly selected fields per sample at 200× magnification. The reported analysis counted EdU-positive and Hoechst-positive cells using ImageJ/Fiji, with investigators blinded to group allocation. EdU positivity was calculated as the number of EdU-positive cells divided by the number of Hoechst-positive cells, multiplied by 100%. Exposure and gain settings were held constant, and samples without EdU labelling were used as negative controls. This counting endpoint requires reconciliation with the fluorescence intensity ratio presented in Fig. 5e.

Intracellular cAMP measurement

After treatment, medium was removed and cells were washed with cold PBS. Cells were lysed in buffer containing 0.5 mM 3-isobutyl-1-methylxanthine to limit cAMP degradation. Intracellular cAMP was measured using a competitive assay (Cayman Chemical, 581001) with sample acetylation. The reported assay range was 0.078–10 pmol/mL, with a sensitivity of 0.1 pmol/mL.

Samples were assayed in duplicate or triplicate, and standard curves were accepted when R^2 was at least 0.99. cAMP concentrations were reported as normalised to total protein or cell number. The reported units were pmol/mg protein or pmol per 10^6 cells, respectively. Forskolin (100 μM) and SQ22536 (10 μM) were listed as positive and inhibitory controls. These normalisation units require reconciliation with the nM scale used in the figures.

PKA-associated assay

The reported PKA assay used a non-radioactive substrate-phosphorylation kit (Abcam, ab139435). Sample aliquots (30 μL) containing equal protein amounts were added to wells coated with a PKA substrate peptide. Protein input was selected within a range of 5–20 μg per well. ATP was added to initiate the reaction, followed by incubation at 30–35 °C for 90 min with mixing every 20 min.

Phosphorylated substrate was detected using a phosphospecific antibody for 60 min at room temperature, followed by an HRP-conjugated secondary antibody. After washing, tetramethylbenzidine was added and the reaction was stopped before absorbance was measured at 450 nm. This colorimetric method requires reconciliation with the fluorescence units reported in Fig. 4b.

Statistical analysis

Statistical analyses were performed using GraphPad Prism 9.0. Data were reported as mean ± standard deviation from at least three independent experiments. The reported tests were Student's t-test for two-group comparisons and one-way analysis of variance followed by Tukey's test for multiple groups. Kaplan–Meier curves were reported as compared using the log-rank test. Pearson correlation was listed for correlation analyses. The significance threshold was $P < 0.05$. Panel-specific sample sizes, experimental units, test sidedness and analyses of repeated measurements require confirmation.

Results

PF reduces cell viability and colony formation and alters migration-associated and sphere-formation endpoints

We first examined PF-associated phenotypic changes in SKOV3 and A2780 cells. After 48 h, CCK-8 measurements decreased across the tested concentration range in both cell lines (Fig. 1a). PF-treated cultures also formed fewer colonies after 14 days (Fig. 1b). Transwell assays showed fewer migrated cells, and wound closure was lower over 24 h (Fig. 1c,d). Total sphere area was also lower following PF treatment (Fig. 1e). These results linked reduced viability and colony formation with changes in migration-associated measurements and sphere area.

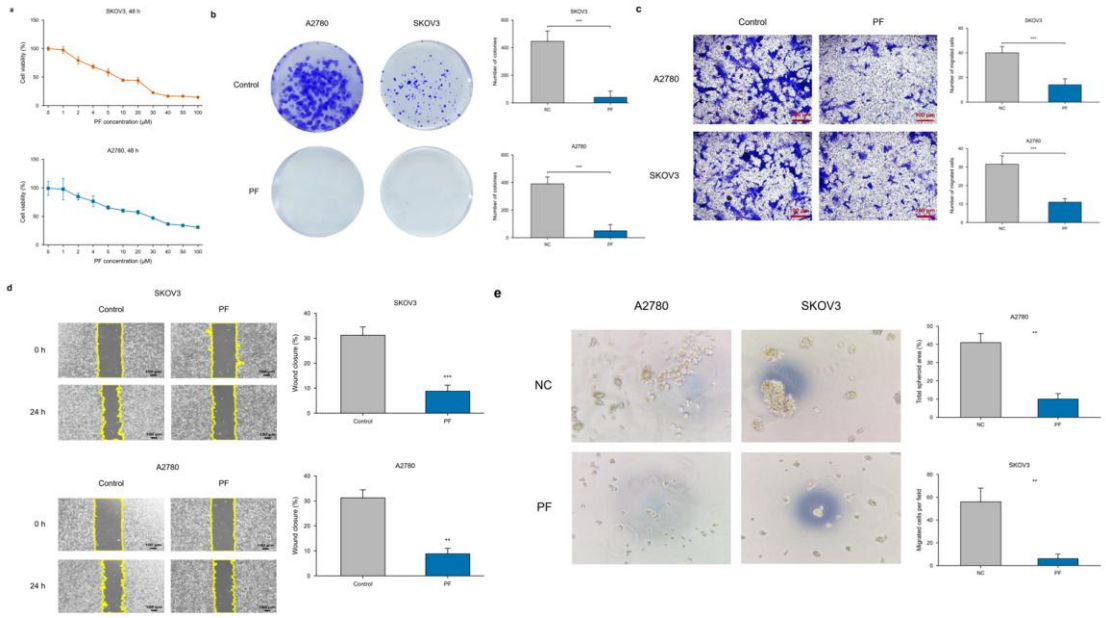

Fig. 1 | PF-associated changes in ovarian cancer cell phenotypes.

(a) CCK-8 viability measurements in SKOV3 and A2780 cells after 48 h of treatment with the indicated PF concentrations. (b) Representative colony-formation images and colony counts after 14 days. Colonies containing more than 50 cells were counted. (c) Representative Transwell images and migrated-cell counts. (d) Representative wound images at 0 and 24 h and corresponding wound-closure measurements. (e) Representative sphere-formation images and total sphere area (%) in A2780 and SKOV3 cells.

NC denotes the control group in the figures; the corresponding treatment vehicle requires assay-specific confirmation.

Expression profiling identifies TM4SF1 as a PF-responsive candidate

We compared expression profiles between control and PF-treated samples to identify candidate molecular responses. The volcano plot showed differential expression, and the heatmap highlighted selected molecules associated with adhesion, extracellular matrix regulation and apoptosis (Fig. 2a,b). KEGG analysis[23] identified enrichment of cAMP, MAPK and cell-cycle pathways (Fig. 2c). We selected TM4SF1 for further examination of protein abundance and cellular distribution. Immunofluorescence images showed its distribution, although the adjacent quantitative labels require clarification (Fig. 2d). Immunoblotting and GAPDH-normalised densitometry showed a lower TM4SF1 signal following PF treatment (Fig. 2e). These observations identified TM4SF1 as a treatment-responsive candidate without establishing a direct PF target.

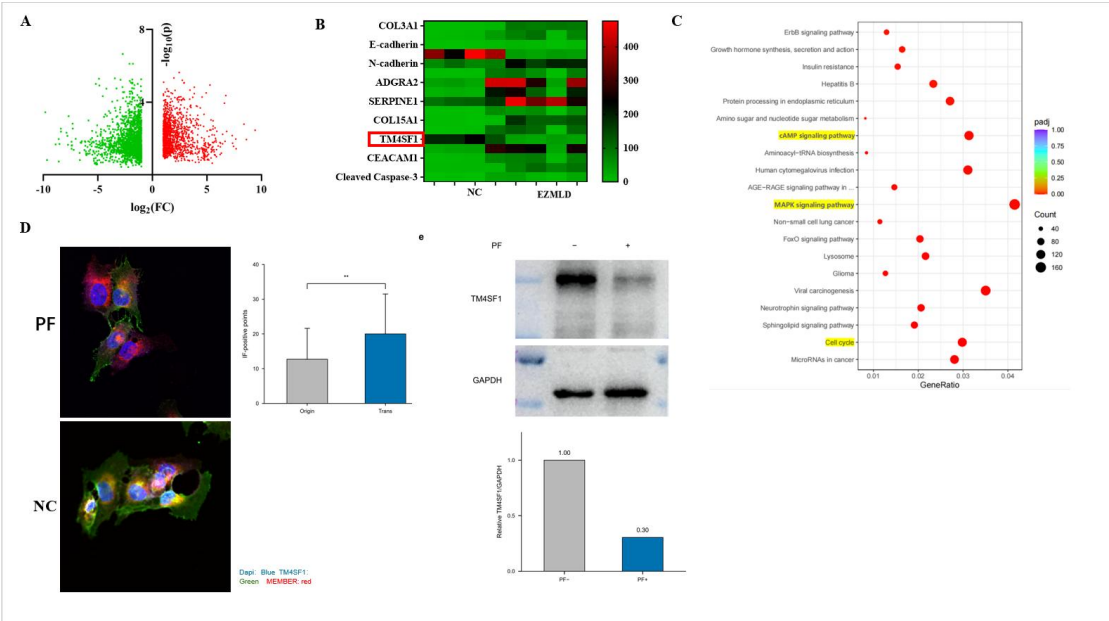

Fig. 2 | Expression profiling and TM4SF1 measurements following PF treatment.

(a) Volcano plot comparing control and PF-treated samples. Axes show $\log_2$(fold change) and $-\log_{10}$(P value). Red and green indicate increased and decreased expression, respectively. (b) Heatmap of selected molecules, with TM4SF1 outlined in red. (c) KEGG pathway enrichment. Dot size indicates gene count, and colour indicates the adjusted P value. Highlighted pathways include cAMP signalling, MAPK signalling and the cell cycle. (d) Representative immunofluorescence images and the accompanying fluorescence summary. TM4SF1, the membrane marker and nuclei are shown in green, red and blue, respectively. (e) Representative TM4SF1 immunoblots and GAPDH-normalised densitometry. PF− and PF+ denote samples without and with PF treatment, respectively.

PF lowers TM4SF1 expression and alters ERK and STAT3 phosphorylation measurements

We next examined TM4SF1 expression at the protein and transcript levels. Immunoblotting showed a lower GAPDH-normalised TM4SF1 signal after PF treatment, accompanied by lower *TM4SF1* mRNA expression (Fig. 3a,b). The p-ERK/ERK ratio was lower in the PF group, whereas the mean p-STAT3/STAT3 ratio was higher (Fig. 3c). The accompanying immunofluorescence summary showed lower green-to-DAPI intensity ratios for TM4SF1 and p-ERK (Fig. 3d). Fractionation measurements showed lower mean normalised TM4SF1 signals in both cytoplasmic and membrane fractions (Fig. 3e). These findings described different responses across signalling measurements, rather than uniform suppression of the ERK and STAT3 pathways.

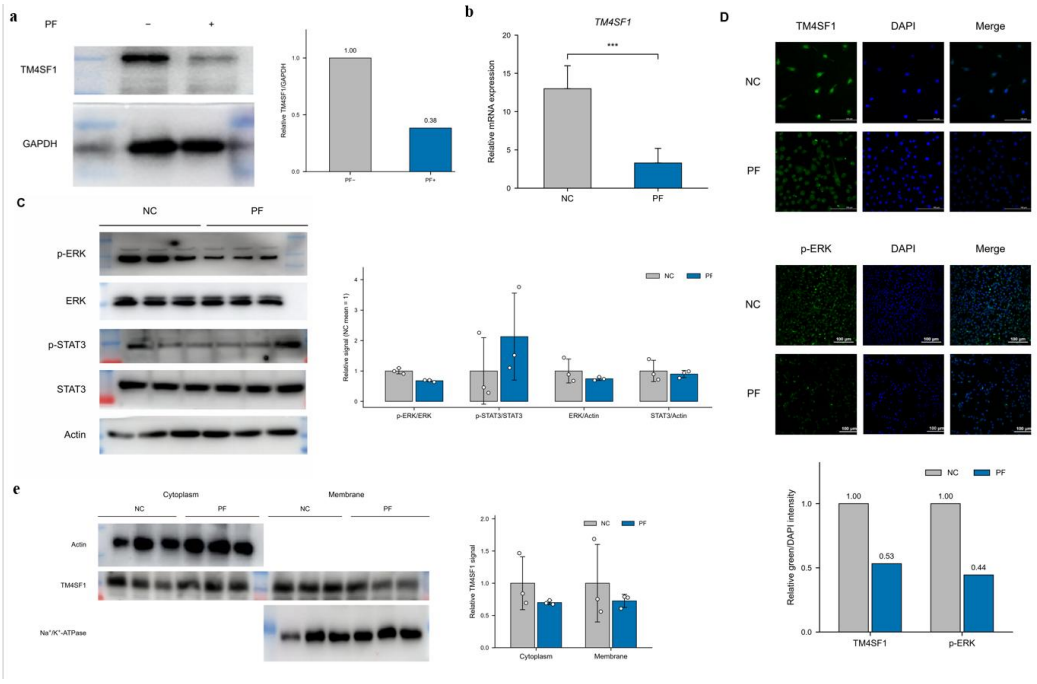

Fig. 3 | TM4SF1 expression and ERK and STAT3 phosphorylation measurements.

(a) Representative TM4SF1 immunoblots and GAPDH-normalised densitometry. (b) *TM4SF1* mRNA expression measured by RT–qPCR. (c) Representative phosphorylated and total ERK and STAT3 immunoblots and densitometry. Phosphorylated proteins were normalised to the corresponding total proteins. Total ERK and STAT3 were normalised to actin. Lanes 1–3 represent NC, and lanes 4–6 represent PF. (d) Representative TM4SF1 and p-ERK immunofluorescence images and green-to-DAPI intensity ratios. Protein signals are green and nuclei are blue. (e) TM4SF1 in cytoplasmic and membrane fractions, normalised to actin and Na^+/K^+-ATPase, respectively. Within each fraction, the first three lanes represent NC and the final three represent PF. Each normalised measurement was expressed relative to its corresponding NC mean.

PF increases cAMP concentrations alongside lower cell-based p-CREB measurements

We assessed intracellular cAMP and related measurements after PF treatment. cAMP concentrations increased across 0, 10, 30 and 50 μM PF in SKOV3 and A2780 cells (Fig. 4a). PKA-associated assay signals showed a similar pattern, although the assay method and plotted units require reconciliation (Fig. 4b). The p-CREB/CREB ratio was lower following PF treatment (Fig. 4c). Immunofluorescence measurements also showed a lower p-CREB-to-DAPI intensity ratio (Fig. 4d). RT–qPCR showed lower *FOS*, *NR4A1*, *IRS2* and *CCND1* mRNA expression (Fig. 4e). Thus, increased cAMP was accompanied by lower cell-based p-CREB measurements and changes in several transcripts.

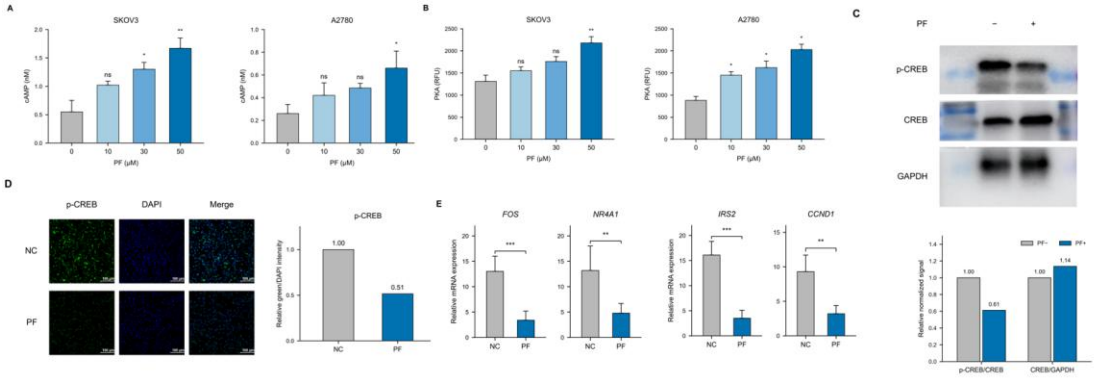

Fig. 4 | Intracellular cAMP and related molecular measurements following PF treatment.

(a) Intracellular cAMP in SKOV3 and A2780 cells treated with the indicated PF concentrations. (b) PKA-associated assay signals, plotted as relative fluorescence units (RFU). (c) Representative p-CREB, CREB and GAPDH immunoblots and densitometry. p-CREB was normalised to CREB, and CREB to GAPDH. Each measurement was expressed relative to the corresponding PF− value. (d) Representative p-CREB immunofluorescence images and green-to-DAPI intensity ratios. p-CREB is green and nuclei are blue. Scale bars, 100 μm. (e) *FOS*, *NR4A1*, *IRS2* and *CCND1* mRNA expression measured by RT–qPCR. PF− and PF+ denote samples without and with PF treatment, respectively.

PF alters apoptosis-associated staining, cell-cycle distribution and EdU fluorescence

We examined apoptosis-associated staining, cell-cycle distribution and EdU fluorescence to characterise further growth-related responses. Flow-cytometric profiles and the accompanying summaries indicated increased apoptosis-associated staining after PF treatment in both cell lines (Fig. 5a). DNA-content analysis showed a lower G0/G1 fraction and a higher G2/M fraction, with little change in S phase (Fig. 5b). Immunoblotting showed higher normalised cleaved caspase-9 and BAX signals, accompanied by lower cyclin D1 and CDK4 signals (Fig. 5c). RT–qPCR showed lower *CDK4*, *CDK2* and *BCL2* expression and higher *BAX* expression (Fig. 5d). The EdU-to-nuclear fluorescence intensity ratio was also lower in the PF group (Fig. 5e). These measurements linked PF treatment to altered cell-cycle distribution and apoptosis-associated responses, together with reduced EdU-associated fluorescence.

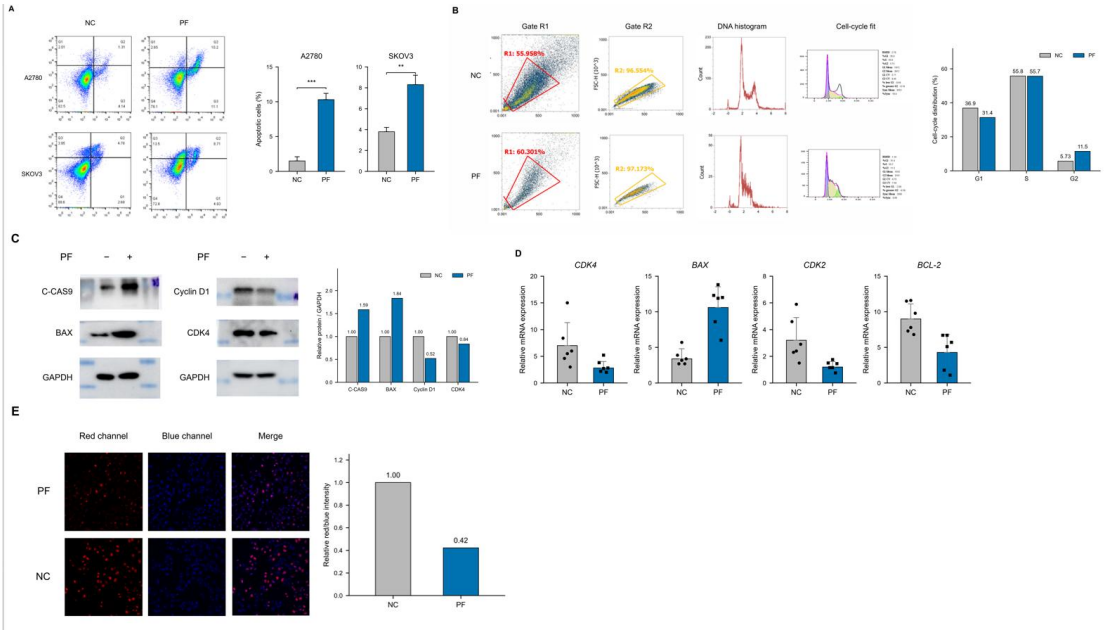

Fig. 5 | Apoptosis-associated staining, cell-cycle distribution and related molecular measurements.

(a) Representative Annexin V–FITC/PI profiles and the accompanying apoptosis-associated summaries in A2780 and SKOV3 cells. (b) Representative gating plots, DNA-content histograms, fitted profiles and cell-cycle proportions. Upper and lower rows represent NC and PF, respectively. The plotted G1 and G2 labels correspond to the G0/G1 and G2/M DNA-content fractions. (c) Representative cleaved caspase-9, BAX, cyclin D1 and CDK4 immunoblots and GAPDH-normalised densitometry. (d) *CDK4*, *BAX*, *CDK2* and *BCL2* mRNA expression measured by RT–qPCR. (e) Representative EdU images and red-to-blue nuclear fluorescence intensity ratios. PF− and PF+ denote samples without and with PF treatment, respectively.

Chemical profiling and constituent comparisons provide a rationale for examining PF

LC–MS profiles were presented for constituents annotated as PF and pachymic acid in the EZMLD preparation (Fig. 6a). These assignments remained tentative because compound identities and extracted-mass information required verification. We then compared cAMP measurements after treatment with PF, wedelolactone, pachymic acid and the compound labelled as nuezhenoside (Fig. 6b). PF-associated cAMP measurements increased across the tested concentration range. The EZMLD 7% comparator produced higher cAMP measurements than the individual-constituent groups under the displayed conditions. Because composition and dose specification differed, these comparisons did not establish relative potency. Together, the chemical and cellular measurements provided a rationale for examining PF as a candidate constituent.

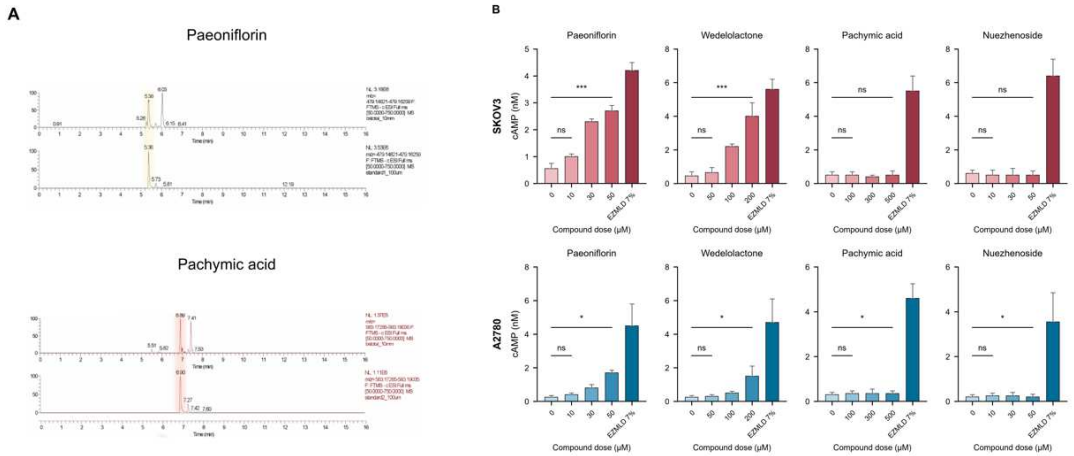

Fig. 6 | Chemical profiling of EZMLD and constituent-associated cAMP measurements.

(a) Chromatographic profiles and extracted-mass information labelled as PF and pachymic acid in the supplied figure. Compound identities, mass-extraction settings and reference-standard assignments require verification. (b) Intracellular cAMP measurements after treatment with PF, wedelolactone, pachymic acid or the compound labelled as nuezhenoside. SKOV3 and A2780 measurements are shown separately. Individual-compound concentrations are expressed in μM. EZMLD 7% is retained as a separate preparation comparator.

Xenograft experiments assess tumour-tissue responses and selected tolerability-related endpoints

We also examined PF-associated responses in an OVCAR3 xenograft model. Tumour volumes were lower in the PF group on day 14, accompanied by smaller excised tumours at the experimental endpoint (Fig. 7a,b). The PF survival curve was shifted to the right (Fig. 7c). Body weight increased over time in both groups (Fig. 7d). Tumour-tissue fluorescence summaries showed lower TM4SF1-to-DAPI and p-CREB-to-DAPI intensity ratios (Fig. 7e). Immunoblotting showed a lower mean TM4SF1/GAPDH ratio, while the mean p-CREB/CREB ratio was close to the control value (Fig. 7f). The mean CREB/GAPDH ratio was slightly lower in the PF group. Serum biochemistry and heart, liver and kidney morphology provided additional descriptive tolerability-related measurements (Fig. 7g,h).

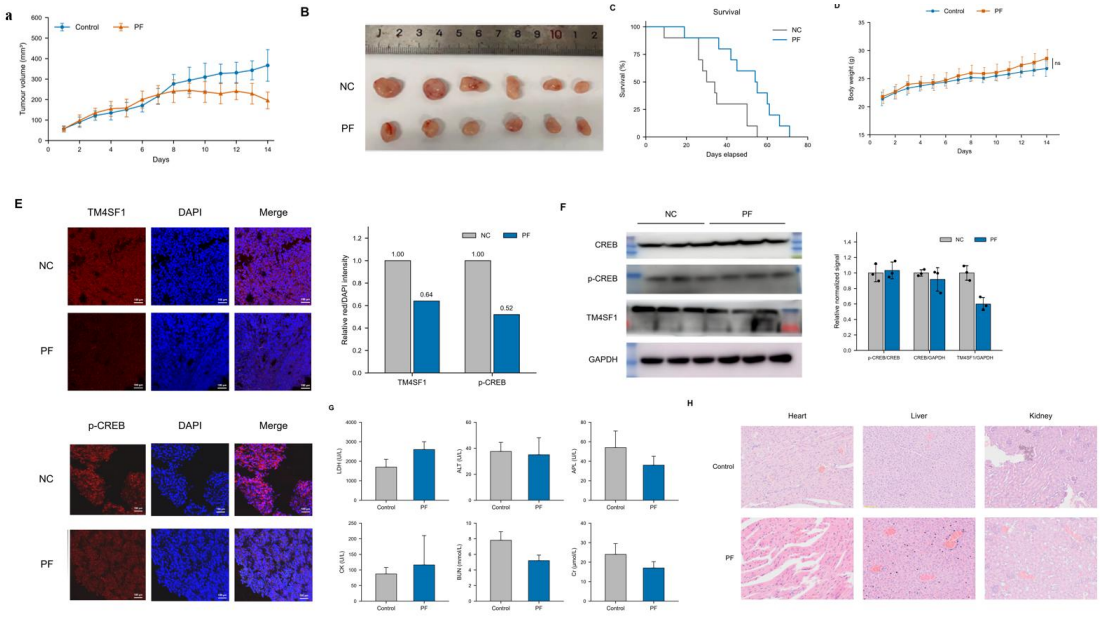

Fig. 7 | Xenograft observations, tumour-tissue measurements and selected tolerability-related endpoints.

(a) Tumour-growth curves during treatment. (b) Excised tumours at the experimental endpoint. (c) Survival curves for control and PF-treated mice. (d) Body-weight trajectories during treatment. (e) Representative tumour-tissue TM4SF1 and p-CREB immunofluorescence images and red-to-DAPI intensity ratios. Protein signals are red and nuclei are blue. Scale bars are labelled 100 μm. (f) Representative CREB, p-CREB, TM4SF1 and GAPDH immunoblots and densitometry. p-CREB was normalised to CREB, and CREB and TM4SF1 to GAPDH. Lanes 1–3 represent NC, and lanes 4–6 represent PF. (g) Serum LDH, ALT, the analyte labelled as APL, CK, BUN and creatinine. (h) Representative H&E-stained heart, liver and kidney sections.

Discussion

PF treatment was associated with reduced viability and colony formation, altered migration-associated measurements and lower sphere area in ovarian cancer cells. These phenotypic responses coincided with lower TM4SF1 expression and higher intracellular cAMP. The study therefore connects a chemically defined intervention with concurrent cellular and molecular responses. It does not establish their causal sequence or identify a single mediator of the phenotypic effects.

The TM4SF1 response is relevant to its established role in ovarian cancer cell motility. Gao and colleagues found that TM4SF1 silencing inhibited migration and invasion without detectable changes in proliferation or cell-cycle distribution[7]. The broader response to PF therefore cannot be assigned to TM4SF1 downregulation alone. Lower TM4SF1 expression may contribute to treatment responses or arise secondarily from changes in cell state or population composition. TM4SF1 depletion and restoration experiments would distinguish these explanations. Demonstrating direct PF binding would require separate biochemical or biophysical evidence.

The cAMP results also resist a simple linear pathway interpretation. Previous ovarian cancer experiments linked cAMP–PKA–CREB signalling to roflumilast-associated tumour inhibition[13]. Here, cAMP increased while cell-based p-CREB/CREB and p-CREB-to-DAPI measurements decreased. Tumour-tissue fluorescence and immunoblotting did not show an equivalent pattern. Spatial organisation of cAMP signalling provides one reason why whole-cell concentrations cannot predict a single downstream response[11,12]. However, the present experiments did not measure local cAMP dynamics or establish this explanation. Matched time courses and validated assays are needed before assigning PKA–CREB activation or inhibition to PF.

Constituent comparisons support examining PF without establishing its predominance within EZMLD. Experimental PF activity has been reported in other cancer models[6], but this does not substitute for ovarian cancer evidence. Higher cAMP measurements in the preparation comparator cannot establish superior potency because exposures and compositions were not matched. Quantitative chemical measurements and constituent depletion or add-back experiments would help define the contribution of PF. Any claim of synergy would require a formal interaction analysis[24].

The xenograft experiments extend the cellular observations to an in vivo setting. Lower tumour volumes and lower TM4SF1 measurements support further investigation of PF-associated responses in tumour tissues. The survival result requires complete reporting of the cohort, event definition and follow-up schedule. Body-weight trajectories, serum biochemistry and selected tissue sections offer preliminary tolerability-related observations. They do not establish systemic safety, clinical efficacy or tolerability in humans. Conclusions should therefore remain restricted to the tested model and exposure.

Several limitations constrain mechanistic interpretation. Direct binding between PF and TM4SF1, and functional regulation of adenylyl cyclase, were not established. The PKA assay

description, fluorescence endpoints and CREB measurements require reconciliation across methods, figures and biological settings. Chemical annotations also need verification against reference standards and original mass-spectrometric records. Changes in proliferation and viability can influence migration and sphere-formation measurements[17,25]. Matched controls are therefore needed to distinguish these effects. Panel-specific replication, complete assay methods and accessible source data would strengthen reproducibility. Controlled perturbation and rescue experiments remain necessary to test whether TM4SF1 or cAMP mediates the observed cellular responses.

Conclusion

PF-associated changes in ovarian cancer cell phenotypes coincided with lower TM4SF1 expression and increased intracellular cAMP. Lower tumour volumes in the xenograft model provided additional evidence of an in vivo response. These observations support further investigation of PF as a candidate constituent of EZMLD. They do not establish a direct molecular target, a causal TM4SF1–cAMP mechanism or a uniform downstream CREB response.

Acknowledgements

Not applicable.

Funding

This study was supported by the National Natural Science Foundation of China (82304907 to G.J. and 82274266 to A.Y.).

The funders had no role in study design, data collection or analysis, manuscript preparation or the decision to publish.

Author contributions

Jing Zhang: investigation, methodology, data curation and writing of the original draft. Yujie Chen: investigation, formal analysis, visualisation and writing of the original draft. Junjie Hong: investigation, validation and manuscript review and editing. Wangang Gong: investigation, resources and manuscript review and editing. Zhangguo Ying: conceptualisation, supervision and manuscript review and editing. Aijun Yu: conceptualisation, supervision, project administration and manuscript review and editing. Guangyi Jiang: formal analysis, visualisation and manuscript review and editing.

Data availability

The datasets used and/or analysed during the current study are available from the corresponding author on reasonable request.

Consent for publication

Consent to publish is not applicable to this study, as it does not contain any identifiable images or data.

Competing interests

The authors declare no competing interests.

Clinical trial registration

Not applicable. This study involved in vitro experiments using established human ovarian cancer cell lines and in vivo experiments in mice; no human participants were involved.

References

1. Lheureux S, Gourley C, Vergote I, Oza AM. Epithelial ovarian cancer. Lancet. 2019;393(10177):1240-1253. doi: 10.1016/S0140-6736(18)32552-2.

2. Patch AM, Christie EL, Etemadmoghadam D, Garsed DW, George J, Fereday S, et al. Whole-genome characterization of chemoresistant ovarian cancer. Nature. 2015;521(7553):489-494. doi: 10.1038/nature14410.

3. Domcke S, Sinha R, Levine DA, Sander C, Schultz N. Evaluating cell lines as tumour models by comparison of genomic profiles. Nat Commun. 2013;4:2126. doi: 10.1038/ncomms3126.

4. Newman DJ, Cragg GM. Natural Products as Sources of New Drugs over the Nearly Four Decades from 01/1981 to 09/2019. J Nat Prod. 2020;83(3):770-803. doi: 10.1021/acs.jnatprod.9b01285.

5. Yang L, Liu J, Zhang J, Shao F, Jin Y, Xing J, et al. Anticancer effects of Erzhimaoling decoction in high-grade serous ovarian cancer in vitro and in vivo. Eur J Med Res. 2024;29(1):405. doi: 10.1186/s40001-024-01968-4.

6. Zheng YB, Xiao GC, Tong SL, Ding Y, Wang QS, Li SB, et al. Paeoniflorin inhibits human gastric carcinoma cell proliferation through up-regulation of microRNA-124 and suppression of PI3K/Akt and STAT3 signaling. World J Gastroenterol. 2015;21(23):7197-7207. doi: 10.3748/wjg.v21.i23.7197.

7. Gao C, Yao H, Liu H, Feng Y, Yang Z. TM4SF1 is a potential target for anti-invasion and metastasis in ovarian cancer. BMC Cancer. 2019;19(1):237. doi: 10.1186/s12885-019-5417-7.

8. Tang Q, Chen J, Di Z, Yuan W, Zhou Z, Liu Z, et al. TM4SF1 promotes EMT and cancer stemness via the Wnt/β-catenin/SOX2 pathway in colorectal cancer. J Exp Clin Cancer Res. 2020;39(1):232. doi: 10.1186/s13046-020-01690-z.

9. Ye L, Pu C, Tang J, Wang Y, Wang C, Qiu Z, et al. Transmembrane-4 L-six family member-1 (TM4SF1) promotes non-small cell lung cancer proliferation, invasion and chemo-resistance through regulating the DDR1/Akt/ERK-mTOR axis. Respir Res. 2019;20(1):106. doi: 10.1186/s12931-019-1071-5.

10. de Rooij J, Rehmann H, van Triest M, Cool RH, Wittinghofer A, Bos JL. Mechanism of regulation of the Epac family of cAMP-dependent RapGEFs. J Biol Chem. 2000;275(27):20829-20836. doi: 10.1074/jbc.M001113200.

11. Zaccolo M, Zerio A, Lobo MJ. Subcellular Organization of the cAMP Signaling Pathway. Pharmacol Rev. 2021;73(1):278-309. doi: 10.1124/pharmrev.120.000086.

12. Bock A, Annibale P, Konrad C, Hannawacker A, Anton SE, Maiellaro I, et al. Optical Mapping of cAMP Signaling at the Nanometer Scale. Cell. 2020;182(6):1519-1530.e17. doi: 10.1016/j.cell.2020.07.035.

13. Gong S, Chen Y, Meng F, Zhang Y, Wu H, Wu F. Roflumilast restores cAMP/PKA/CREB signaling axis for FtMt-mediated tumor inhibition of ovarian cancer. Oncotarget. 2017;8(68):112341-112353. doi: 10.18632/oncotarget.22866.

14. Dimitrova N, Nagaraj AB, Razi A, Singh S, Kamalakaran S, Banerjee N, et al. InFlo: a novel systems biology framework identifies cAMP-CREB1 axis as a key modulator of platinum resistance in ovarian cancer. Oncogene. 2017;36(17):2472-2482. doi: 10.1038/onc.2016.398.

15. Ishiyama M, Miyazono Y, Sasamoto K, Ohkura Y, Ueno K. A highly water-soluble disulfonated tetrazolium salt as a chromogenic indicator for NADH as well as cell viability. Talanta. 1997;44(7):1299-1305. doi: 10.1016/s0039-9140(97)00017-9.

16. Franken NA, Rodermond HM, Stap J, Haveman J, van Bree C. Clonogenic assay of cells in vitro. Nat Protoc. 2006;1(5):2315-2319. doi: 10.1038/nprot.2006.339.

17. Liang CC, Park AY, Guan JL. In vitro scratch assay: a convenient and inexpensive method for analysis of cell migration in vitro. Nat Protoc. 2007;2(2):329-333. doi: 10.1038/nprot.2007.30.

18. Schneider CA, Rasband WS, Eliceiri KW. NIH Image to ImageJ: 25 years of image analysis. Nat Methods. 2012;9(7):671-675. doi: 10.1038/nmeth.2089.

19. Livak KJ, Schmittgen TD. Analysis of relative gene expression data using real-time quantitative PCR and the $2^{-\Delta\Delta CT}$ method. Methods. 2001;25(4):402-408. doi: 10.1006/meth.2001.1262.

20. Vermes I, Haanen C, Steffens-Nakken H, Reutelingsperger C. A novel assay for apoptosis. Flow cytometric detection of phosphatidylserine expression on early apoptotic cells using fluorescein labelled Annexin V. J Immunol Methods. 1995;184(1):39-51. doi: 10.1016/0022-1759(95)00072-i.

21. Pozarowski P, Darzynkiewicz Z. Analysis of cell cycle by flow cytometry. Methods Mol Biol. 2004;281:301-311. doi: 10.1385/1-59259-811-0:301.

22. Salic A, Mitchison TJ. A chemical method for fast and sensitive detection of DNA synthesis in vivo. Proc Natl Acad Sci U S A. 2008;105(7):2415-2420. doi: 10.1073/pnas.0712168105.

23. Kanehisa M, Furumichi M, Sato Y, Kawashima M, Ishiguro-Watanabe M. KEGG for taxonomy-based analysis of pathways and genomes. Nucleic Acids Res. 2023;51(D1):D587-D592. doi: 10.1093/nar/gkac963.

24. Foucquier J, Guedj M. Analysis of drug combinations: current methodological landscape. Pharmacol Res Perspect. 2015;3(3):e00149. doi: 10.1002/prp2.149.

25. Pastrana E, Silva-Vargas V, Doetsch F. Eyes wide open: a critical review of sphere-formation as an assay for stem cells. Cell Stem Cell. 2011;8(5):486-498. doi: 10.1016/j.stem.2011.04.007.

Supplementary Files

This is a list of supplementary files associated with this preprint. Click to download.

- Westernblotting.pdf